Received: 20 July 2022 | Revised: 27 August 2022 | Accepted: 27 August 2022

DOI: 10.1002/rcm.9386

RESEARCH ARTICLE

Rapid Communications in Mass Spectrometry WILEY

Developing transmission mode for infrared matrix-assisted laser desorption electrospray ionization mass spectrometry imaging

Alena N. Joignant[1] | Hongxia Bai[1,2] | Jacob P. Guymon[3] | Kenneth P. Garrard[1,2,3] | Mark Pankow[3] | David C. Muddiman[1,2]

[1]FTMS Laboratory for Human Health Research, Department of Chemistry, North Carolina State University, Raleigh, North Carolina, USA

[2]Molecular Education, Technology and Research Innovation Center, North Carolina State University, Raleigh, North Carolina, USA

[3]Precision Engineering Consortium, Department of Mechanical and Aerospace Engineering, North Carolina State University, Raleigh, North Carolina, USA

Correspondence
D. C. Muddiman, FTMS Laboratory for Human Health Research, Department of Chemistry, North Carolina State University, Raleigh, NC.
Email: dcmuddim@ncsu.edu

Funding information
North Carolina State University; NIH Molecular Biotechnology Training Program, Grant/Award Number: 5T32GM133366-03; National Institute of Health, Grant/Award Number: R01GM087964

Rationale: The development and characterization of the novel NextGen infrared matrix-assisted laser desorption electrospray ionization (IR-MALDESI) source catalyzed new advancements in IR-MALDESI instrumentation, including the development of a new analysis geometry.

Methods: A vertically oriented transmission mode (tm)-IR-MALDESI setup was developed and optimized on thawed mouse tissue. In addition, glycerol was introduced as an alternative energy-absorbing matrix for tm-IR-MALDESI because the new geometry does not currently allow for the formation of an ice matrix. The tm geom was evaluated against the optimized standard geometry for the NextGen source in reflection mode (rm).

Results: It was found that tm-IR-MALDESI produces comparable results to rm-IR-MALDESI after optimization. The attempt to incorporate glycerol as an alternative matrix provided little improvement to tm-IR-MALDESI ion abundances.

Conclusions: This work has successfully demonstrated the adaptation of the NextGen IR-MALDESI source through the feasibility of tm-IR-MALDESI mass spectrometry imaging on mammalian tissue, expanding future biological applications of the method.

1 | INTRODUCTION

Mass spectrometry imaging (MSI) provides the spatial distribution of molecules in a sample with high specificity, which is beneficial especially in the analysis of biospecimens.[1] In ablation-based MSI, the most common analysis method is to direct the laser to the top surface of a sample, commonly known as reflection mode (rm). One primary disadvantage of rm MSI is possible obstruction of the plume of the ablated sample by laser optics or post-ionization method. At short working distances, this can result in the loss of desorbed analyte and make optical elements dirty. Therefore, post-ionization techniques and laser-focusing lens are typically spatially restricted in a reflection geometry.

Transmission mode (tm, also referred to as transmission geometry) is not new to ablation-based MS techniques. Early analyses of materials via laser desorption microprobes often used tm long before the advent of matrix-assisted laser desorption/ionization (MALDI), one of the prevailing ablation-based ionization methods.[2]

Alena N. Joignant and Hongxia Bai contributed equally to this study.

Transmission mode involves excitation energy transmitting through a wavelength-transparent substrate (e.g., glass microscope slide) such that the desorbed material is ejected away from the energy source along the optical axis. Desorption begins on the substrate–sample interface, and the desorbed material is then ejected through the remainder of the sample as opposed to being ejected from the surface as in rm. Therefore, tissue must be fully ablated in tm, limiting the thickness of samples that can be analyzed.[3,4] The first use of tm-MSI in the analysis of biospecimens showed that single laser shots with fluence below 1.0 mJ/cm^2 in transmission geometry provided sufficient ion abundances at acceptable analysis speed and spatial resolution.[5]

Infrared matrix-assisted laser desorption electrospray ionization (IR-MALDESI) is a hybrid ionization technique that is especially suited for MSI and has operated in rm since the advent of MALDESI in 2006.[6] In IR-MALDESI, a 2970 nm laser is fired at the sample, sending desorbed neutrals into an orthogonal electrospray plume to be post-ionized. A specific advantage includes the resonant absorption of the 2970 nm laser by endogenous or externally applied water/ice, eliminating the need for organic matrices.[7] The current IR-MALDESI optical path contains a vertically directed laser beam down into the source enclosure. In an effort to leave this path unaltered, the specimen slide must be oriented upside down above the stage in tm. This is useful, as it allows gravity to assist the transfer of ablated material down toward the post-ionization mechanism and prevents neutrals from falling back to the sample, which could be an issue in rm.[8] In addition, this could allow us to collect any neutrals that fall onto the original stage for further analysis. Unfortunately, tm-IR-MALDESI does not allow for the formation of an ice matrix, because the sample cannot currently lay directly on the Peltier-cooled IR-MALDESI stage. Specific advantages of the ice matrix in IR-MALDESI include higher signal abundance (more than threefold) and smaller ablation diameters.[7,9] The lack of the ability to produce an ice matrix suggests the possible need for an alternative energy-absorbing matrix. Our recent work has found that glycerol is an effective energy-absorbing matrix relative to the standard ice matrix and produces improved spatial resolution, with no significant change in ion abundance in rm.[10] Therefore, glycerol was used in this work in the tm setup. The study by Kibbe et al found that spraying glycerol on top of the sample provided optimal results, suggesting the need to reverse the matrix-sample order for tm-IR-MALDESI because the laser fires through the back of the sample. Thus, the sample was mounted on top of the glycerol matrix in the present work for better laser–matrix interaction. To our knowledge, it is currently unknown how the application of glycerol changes plume dynamics relative to the ice matrix. The following proof-of-concept work seeks to (a) develop tm-IR-MALDESI and (b) study the impact of a glycerol energy-absorbing matrix in tm. The work shows that IR-MALDESI can accommodate a vertically oriented tm geometry without sacrificing the benefits of rm, specifically the motion control and imaging control software used by the original rm translation stage.

2 | EXPERIMENTAL

2.1 | Materials

HPLC-grade acetonitrile, water, formic acid, glycerol, precleaned microscope slides, glass coverslips, and Arcturus HistoGene staining solution were purchased from Fisher Scientific (Nazareth, PA, USA). Laser alignment paper was purchased from ZAP-IT (Concord, NH, USA).

2.2 | Sample preparation

Mouse liver tissue was used for this study to minimize natural variability, because liver is relatively chemically homogenous at the spatial resolution of IR-MALDESI.[11] Healthy wild-type mouse liver specimens were provided by the Ghashghaei Lab in the College of Veterinary Medicine at North Carolina State University (Raleigh, NC, USA). Animal husbandry practices were performed in accordance with the North Carolina State University Institutional Animal Care and Use Committee and the Institute for Laboratory Animal Research Guide. The specimens were promptly frozen and kept at −80°C until cryosectioning. On experiment days, the liver was cryosectioned at −20°C using a Leica CM1950 cryostat (Buffalo Grove, IL, USA). Each 20 μm section was thaw-mounted onto a precleaned microscope slide and kept at −20°C until further analysis.

2.3 | Transmission mode infrared matrix-assisted laser desorption electrospray ionization

Preliminary tm-IR-MALDESI studies were conducted on the current IR-MALDESI source, which has been previously described.[12] Preliminary tm-IR-MALDESI experiments included stilts constructed from molded plastic building blocks (data not shown). The present work focuses on tm-IR-MALDESI performed on the novel NextGen source.[13] A transmission mode slide holder was customized for the NextGen source in the Precision Engineering Consortium at North Carolina State University. An aluminum block was cut to shape a single arm that extends past the sample stage and above the MS inlet. A 3D model of the arm is provided with this work (see Supporting Information, DATA S1). A microscope slide clip was attached to a small aluminum piece to clamp the slide and thaw-mounted sample upside down. Each component was precision engineered to ensure that the microscope slide remains level with respect to the translation stage. The slide holder was designed to screw into the aluminum plate of the motorized stage of the NextGen source, as this piece was also precision engineered to be level. Two set pins ensure that the arm can be removed and replaced with little variability. The motorized stage was controlled by RastirZ, which together allowed the user to define specific z-heights to an accuracy within 1 μm.[14] The precleaned glass microscope slides were not completely transparent at 2.97 μm and had an approximate energy transmission of 80%, as measured using a

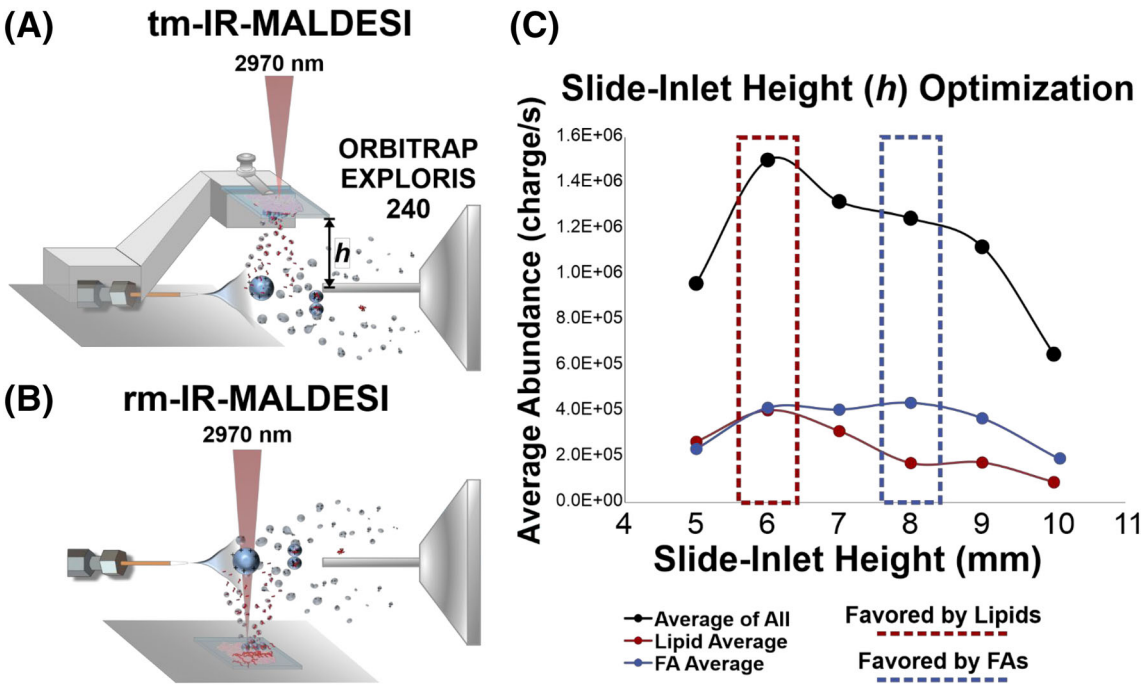

FIGURE 1 A, Schematic of tm-IR-MALDESI. A 2970 nm laser ablates sample downward through a glass microscope slide. A plume of desorbed neutrals meet an orthogonal electrospray plume. Ions travel into the inlet of an Orbitrap Exploris 240. B, Schematic of rm-IR-MALDESI. C, Results of stage height optimization. The averaged curve includes cholesterol ($[M\text{-}H_2O+H^+]^+$, *m/z* 369.3516), lipids, and fatty acids (FAs). The lipids include $C_{42}H_{81}NO_8P + H^+$ (*m/z* 758.5694), $C_{39}H_{74}NO_8P + H^+$ (*m/z* 716.5225), and $C_{46}H_{84}NO_8P + H^+$ (*m/z* 810.6007). The fatty acids include $C_{22}H_{32}O_2 + H^+$ (*m/z* 329.2475), $C_{20}H_{32}O_2 + H^+$ (*m/z* 305.2475), and $C_{18}H_{32}O_2 + H^+$ (*m/z* 281.2475). tm-IR-MALDESI, transmission mode infrared matrix-assisted laser desorption electrospray ionization [Color figure can be viewed at wileyonlinelibrary.com]

Nova II laser power meter with a 3A-P laser thermal power sensor (Ophir Optronics, Jerusalem, Israel). All laser energy in this work was reported after considering this energy transmission. The laser energy applied per shot can be adjusted by changing the number of pulses per laser burst (p/b) at a pulse rate of 10 kHz.[15] Due to the 20% energy loss through the glass substrate, it is not possible to exactly match the energy in tm- and rm-IR-MALDESI. For samples using a glycerol matrix, a 50% glycerol solution (40% methanol in water) was evenly coated onto a precleaned glass microscope slide using a pneumatic TM-Sprayer (HTX Technologies, Chapel Hill, NC, USA) with a flow rate of 10 μL/min, pressure at 10 psi, crisscross pattern with 500 mm/min velocity, and four passes. Considering these parameters, ~50 μL of glycerol matrix was applied to an entire slide, or 0.667 μL per 5 × 5 mm region of interest (ROI). The cryosectioned mouse liver tissue was then thaw-mounted onto the glycerol layer. Because the laser was fired through a transparent substrate to the back of the sample, the energy-absorbing matrix was placed in between the slide and the tissue to maximize IR absorption and thus facilitate sample ablation. This order is directly inverse to that of rm-IR-MALDESI.[10]

The electrospray solvent comprised an acetonitrile–water (60:40, v/v) solution modified with an additional 0.2% formic acid.[16] The flow rate of the electrospray solvent was maintained at either 1.5 or 2 μL/min across two experiment days. A high voltage (3500–3900 V) was applied to the emitter tip to create a stable electrospray plume. During a tm analysis, the slide was installed upside down on the slide holder, and the clamp was tightened. The laser burst was fired through the glass microscope slide, through the sample, and downwards toward the electrospray axis. MS was conducted within an *m/z* mass range of 200–1000 in positive ionization mode at a resolving power of 240 000 (full width at half maximum at *m/z* 200) using an Orbitrap Exploris 240 mass spectrometer (Thermo Fisher Scientific, Bremen, Germany). The ion accumulation time was set to 15 ms to maximize the biological ion flux for imaging, and automatic gain control was disabled. EASY-IC (fluoranthene, *m/z* 202.0782) lock mass was applied to achieve mass measurement accuracy within 2.5 ppm. The thawed tissue samples were immediately stained after analysis and preserved under a coverslip using Permount. When staining tissue ablated with a glycerol matrix, the staining procedure was altered slightly to prevent the loss of tissue. This involved gently pipetting ethanol solution over the tissue as opposed to submerging it. The samples were visualized by optical microscopy using a Leica LMD7000 (Leica Microsystems, Buffalo Grove, IL, USA).

2.4 | Data analysis

First, the RAW files were converted to mzML format using MS Convert by ProteoWizard and then to imzML format via imzMLConverter.[17,18] These files were analyzed in MSiReader v1.03q

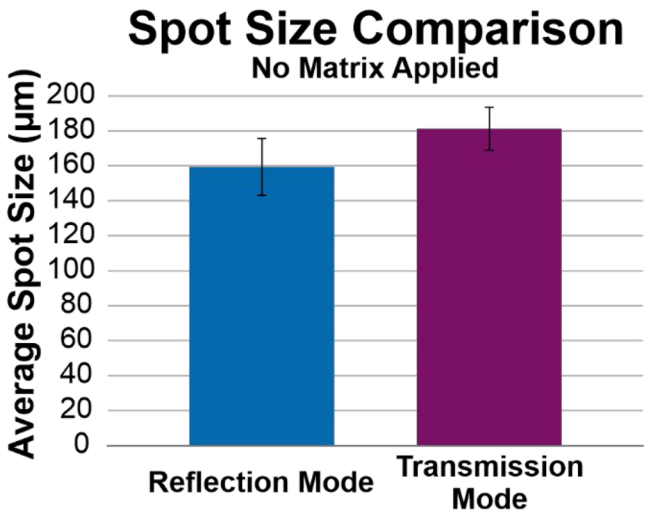

FIGURE 2 Spot size comparison of reflection mode and transmission mode on thawed murine liver tissue (20 µm), with no matrix applied. Reflection mode produced spots at 159 ± 16.3 µm at a laser energy of 1.3 mJ, and transmission mode produced spots at 181 ± 12.3 µm at a laser energy of 1.5 mJ. Error bars represent a 95% confidence interval [Color figure can be viewed at wileyonlinelibrary.com]

for further data visualization and analysis.[19,20] These heatmaps were generated using the cividisblack colormap, which is scientifically derived to be linearly perceptive and color vision deficiency friendly.[21,22] Annotations were acquired in METASPACE using the LipidMaps database at a 20% false discovery rate.[23] These annotations were filtered by MSiPeakfinder with the following criteria: (a) the annotation must be present in amounts greater than 60% of the sample and less than 20% of the ambient electrospray or (b) if an annotation is present in amounts more than 20% of the background, its on-tissue abundance must be at least twice the ambient electrospray abundance.

3 | RESULTS AND DISCUSSION

Using the precision-engineered slide holder shown in Figure 1A, the incorporation of tm into IR-MALDESI was relatively seamless and did not require any alteration to laser optics. Figure S1 (supporting information) shows the slide holder in the NextGen source enclosure, with all components labeled. As shown, the glass slide was clamped to the holder, with the specimen hanging upside down. There was no concern with the specimen falling off the glass slide, nor was this observed, because the samples were thaw-mounted before analysis.

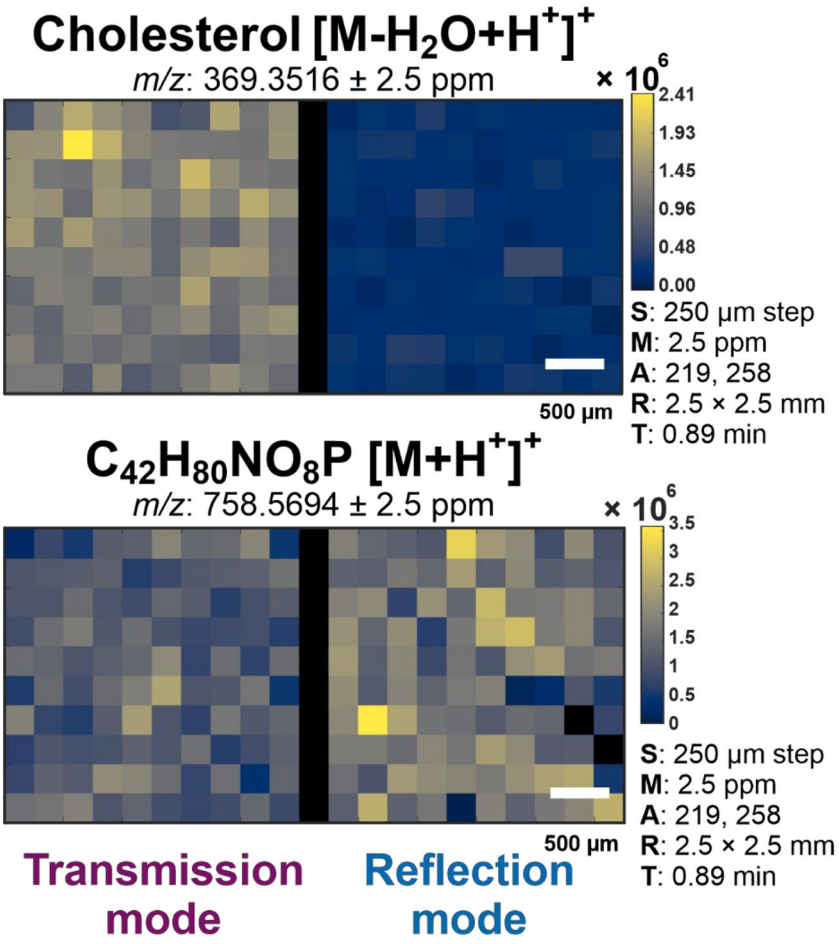

FIGURE 3 Comparison of (left) tm-IR-MALDESI and (right) rm-IR-MALDESI heatmaps of cholesterol ($[M\text{-}H_2O + H^+]^+$ *m/z* 369.3516) and glycerophospholipid $C_{42}H_{81}NO_8P$ ($[M + H^+]^+$ *m/z* 758.5694), with no matrix applied. Included is the SMART acronym: step size, mass measurement accuracy tolerance, number of annotations, region of interest, and time of acquisition. IR-MALDESI, infrared matrix-assisted laser desorption electrospray ionization; rm, reflection mode; tm, transmission mode [Color figure can be viewed at wileyonlinelibrary.com]

3.1 | Optimization of sample-inlet height

Preliminary tests indicated that while comparably complete ablation was observed, ion abundances were relatively low when compared to rm. This was attributed primarily to the fact that no optimization was performed on the tm stage geometry, specifically the distance between the sample and the electrospray axis for post-ionization. In similar ionization methods where the electrospray plume was orthogonal to the optical axis, it was observed that a longer distance between the sample and electrospray axis was optimal.[24] Therefore, the slide-inlet height (*h*) was optimized across 5, 6, 7, 8, 9, and 10 mm using the motorized *z*-axis stage. Figure 1B shows the results of this optimization, indicating that the averaged abundance of lipids, fatty acids, and cholesterol reached maximums at 6 mm, the optimal slide-inlet height. It was observed that fatty acids behaved differently from the larger lipids during optimization. A plausible reason for the separation of these molecular groups includes differences in hydrophobicity between the smaller fatty acids and larger lipids, which had a strong preference for 6 mm. Although fatty acids do not show as much preference as the larger glycerophospholipids, they show a slight maximum average abundance at 8 mm rather than the optimal 6 mm. This optimized value is 1 mm longer than the optimal slide-inlet height of rm-IR-MALDESI (5 mm), possibly due to the different effects of the gravity on the ablation plume.

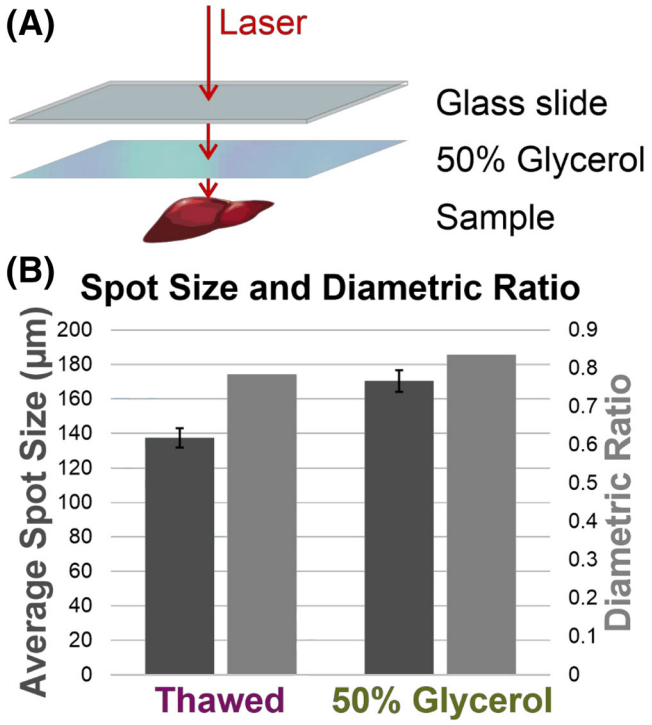

FIGURE 4 A, The order of ablation. A 50% glycerol solution was sprayed on a glass slide so that it was ablated by the laser first in the tm orientation. B, Spot size comparison of tm-IR-MALDESI on 20 µm thawed murine liver tissue and tissue with a 50% glycerol matrix. Thawed tissue spots were 137 ± 5.6 µm, and glycerol matrix spots were 186 ± 6.3 µm, both at a laser energy of 1.6 mJ. Error bars represent a 95% confidence interval. tm-IR-MALDESI, transmission mode infrared matrix-assisted laser desorption electrospray ionization [Color figure can be viewed at wileyonlinelibrary.com]

3.2 | Comparison to rm-IR-MALDESI

It is worth noting that, due to some energy loss through the glass slide, it is not possible for both tm and rm samples to use the same laser energy. For this comparison, tm-IR-MALDESI was performed using 3 p/b (~1.5 mJ after the glass slide), and rm-IR-MALDESI used 2 p/b (~1.2 mJ). Both analyses were conducted without a matrix. Spot size data indicate that tm results in comparable ablation areas to rm at similar fluence: ~5.9 and 6.0 J/cm^2, respectively (Figure 2). Optical images of the tissue post-analysis are shown in Figure S2 (supporting information). In addition, comparable ion abundances were observed between rm-IR-MALDESI and tm-IR-MALDESI (Figure S3 [supporting information]). Slightly fewer lipid classes were

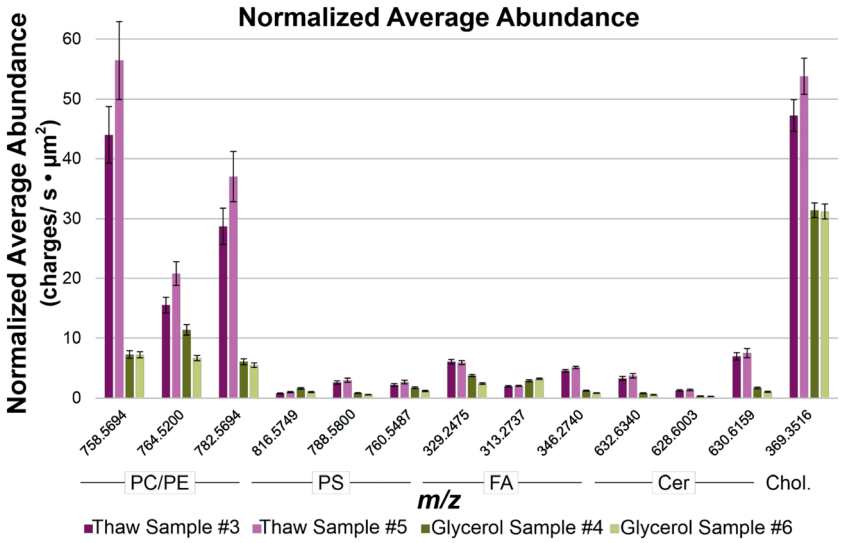

FIGURE 5 Bar graph comparing average ion abundances of representative annotations observed using tm-IR-MALDESI without a matrix and glycerol tm-IR-MALDESI: $C_{42}H_{80}NO_8P + H^+$, $C_{41}H_{76}NO_8P + Na^+$, $C_{44}H_{80}NO_8P + H^+$, $C_{44}H_{82}NO_{10}P + H^+$, $C_{43}H_{82}NO_9P + H^+$, $C_{41}H_{78}NO_9P + H^+$, $C_{22}H_{32}O_2 + H^+$, $C_{19}H_{36}O_3 + H^+$, $C_{22}H_{35}NO_2 + H^+$, and $C_{27}H_{46}O\text{-}H_2O + H^+$. Error bars represent a95% confidence interval. Average abundances were background-subtracted and normalized to the average area ablated by each sample. All samples were of equal thickness (20 µm) and cut from the same mouse liver specimen. tm-IR-MALDESI, transmission mode infrared matrix-assisted laser desorption electrospray ionization [Color figure can be viewed at wileyonlinelibrary.com]

annotated in tm relative to the NextGen source, but cholesterol was observed at much higher abundance. Fatty acid ion abundances were comparable between the two geometries. These data were acquired at a 6 mm slide-inlet height after optimization, showing the benefit of the slide-inlet height optimization for ion abundances.

Figure 3 isolates cholesterol and glycerophospholipid $C_{42}H_{80}NO_8P + H^+$ heatmaps for comparison, showing comparable ion images and confirming the higher cholesterol abundance observed in the raw spectra in tm and slightly higher lipid abundance in rm. Overall, it was determined that tm produced comparable results to rm-IR-MALDESI on thawed tissue.

3.3 | Investigation of glycerol matrix for tm-IR-MALDESI

The inability to apply an ice matrix in tm motivated the attempt of an alternative glycerol matrix, which was previously shown to be advantageous in rm-IR-MALDESI at a 50% concentration (v/v).[10] Figure 4A shows the order of the glass slide, glycerol matrix, and sample in tm-IR-MALDESI. Because a matrix is the first thing that is ablated in rm-IR-MALDESI, the glycerol solution was sprayed on the glass slide before thaw-mounting the tissue for tm-IR-MALDESI. The 50% glycerol matrix was compared directly to tm-IR-MALDESI without a matrix (thawed tissue). The spot size that resulted from the application of the glycerol matrix was 186 ± 6.3 μm, substantially larger than that of the thawed tissue (Figure 4B). The variability (percentage relative standard deviation [%RSD]) of these measures was 13% and 11%, respectively. The energy absorption of the glycerol matrix may affect the boundaries of the ablation area where the laser energy of the Gaussian beam nears the ablation threshold, resulting in larger spot sizes. Optical images of the tissue post-analysis are shown in Figure S4 (supporting information). It was observed that the boundaries of the ablation areas under glycerol seem much less regular than those on the thawed tissue. Although efforts were made to avoid displacing the tissue during staining, the dissolution of glycerol in ethanol post-analysis may result in changes in the outlines of the spots, though this was not expected to change spot size. The diametric ratio (*d*), a measure of circularity as defined by Equation (1), was higher using the glycerol matrix. *b* and *a* represent the two radii of an ellipse, with *b* being the shorter of the two such that a perfect circle occurs at a maximum diametric ratio of one.

$$\text{Diametric ratio } (d) = \frac{b}{a} \quad \text{where } b \le a \tag{1}$$

The observed difference in spot size necessitates normalization to ablation volume when comparing average abundances between the two conditions. Figure 5 shows the normalized average abundances across all 400 scans for 10 representative annotations observable

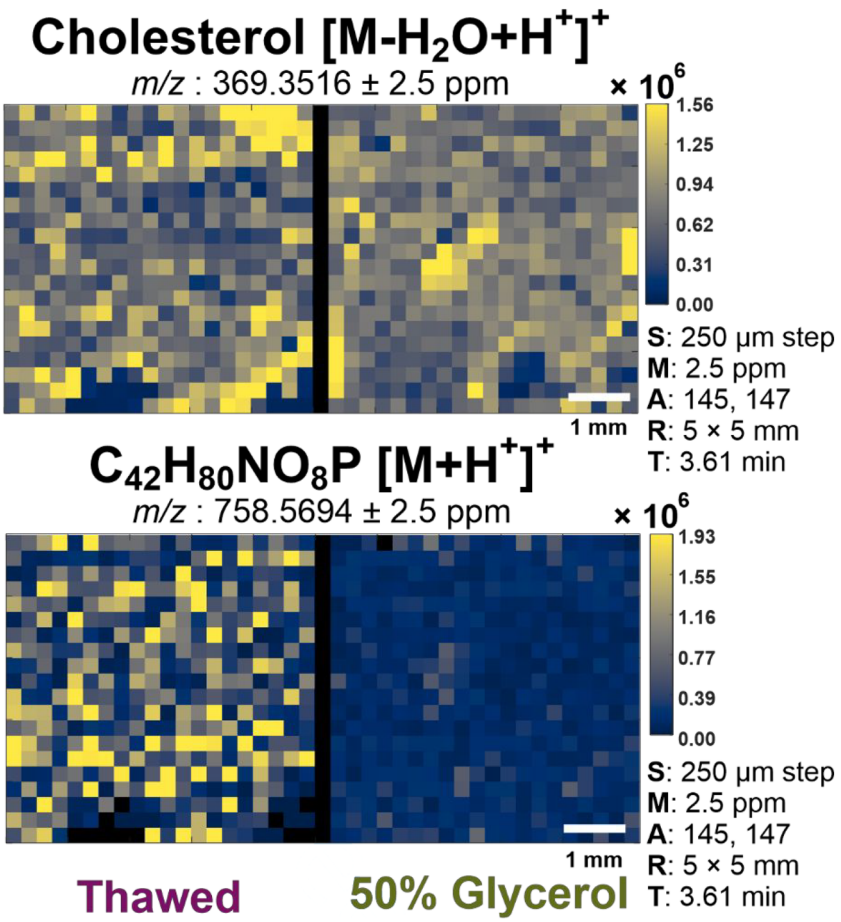

FIGURE 6 Nonnormalized heatmap comparisons between (left) thawed and (right) 50% glycerol matrix conditions of cholesterol ($[M\text{-}H_2O + H^+]^+$ *m/z* 369.3516) and glycerophospholipid $C_{42}H_{81}NO_8P$ ($[M + H^+]^+$ *m/z* 758.5694) [Color figure can be viewed at wileyonlinelibrary.com]

across all samples. Data suggest that there is no improvement in ion abundance in tm-IR-MALDESI using a glycerol matrix. Figure S5 (supporting information) shows a comparison of the raw averaged spectra. Some hotspots (single scans of abnormally high ion abundance) were observed in the thawed tissue ion images, which could have contributed to the drastic differences in certain lipid classes (e.g., PC, Cer). Figure S6 (supporting information) shows that the %RSD was higher in these thawed samples, indicating that the glycerol matrix results in lower variability. To evaluate whether this played a large-enough role to create the higher abundances in thawed tissue, cholesterol and glycerophospholipid $C_{42}H_{80}NO_8P + H^+$ heatmaps were compared at 95% hotspot removal (Figure 6). This comparison illustrates that thawed tissue without a glycerol matrix still resulted in higher ion abundances even after the removal of the hotspots. It was also observed that the %RSD of the fatty acids is smaller than that of larger lipids. This difference could be due to differences in optimization or laser ablation efficiency. It is possible that the factors that improved the rm-IR-MALDESI ion abundances with the addition of 50% glycerol matrix are not at play in tm, and future work may elucidate this discrepancy.

Though the glycerol matrix did not show improvement to tm-IR-MALDESI in this work, the results are promising in that they show comparable results between tm- and rm-IR-MALDESI on thawed tissue, to which the new geometry is currently limited. The decrease in signal variation observed using the glycerol matrix indicates that it or a similar matrix may still be beneficial to tm-IR-MALDESI with future development. Any future work on improving tm-IR-MALDESI would therefore only be to improve the application breadth of the technique. This could include incorporating coverslips as an alternative transparent substrate for higher energy transmission, investigating alternative matrices apart from glycerol for higher energy absorption, or identifying the changes in plume dynamics that result from using a glycerol matrix to optimize tm-IR-MALDESI. In future studies, ablated neutrals that fall past the electrospray axis could be collected or retrieved from the original stage for further analysis, including liquid chromatography tandem mass spectrometry (LC–MS/MS) for omics analysis or structure elucidation. In addition, tm-MSI allows for high-magnification laser optics that require shorter working distances to the target, previously impossible in rm. By avoiding the spatial complications of rm, tighter laser focusing leads to much higher spatial resolution in tm.[24,25] We have yet to capitalize on the ability to place high-magnification optics before the glass slide, such as a reflective objective or a spherical lens with shorter focal length than that previously described. With such incorporation, tm-IR-MALDESI is expected to provide better spatial resolution for fine anatomic structure elucidation.

4 | CONCLUSION

Overall, the development and initial optimization of tm-IR-MALDESI MSI for mammalian tissue was successful, and results indicate that it is comparable to rm-IR-MALDESI on thawed tissue. Although attempts to improve tm-IR-MALDESI using glycerol as an alternative matrix did not result in significant improvement, the work presented here broadens applications and continued innovation of the NextGen IR-MALDESI source.

ACKNOWLEDGMENTS

The authors thank the National Institute of Health (R01GM087964) and the NIH Molecular Biotechnology Training Program (5T32GM133366-03) for their financial support. This work was completed in the Molecular Education, Technology and Research Innovation Center (METRIC) at North Carolina State University.

CONFLICT OF INTEREST

The authors declare no conflicts of interest.

DATA AVAILABILITY STATEMENT

Data will be placed in METASPACE and made public upon publication at https://metaspace2020.eu/project/joignant-tm-2022.

ORCID

David C. Muddiman https://orcid.org/0000-0003-2216-499X

REFERENCES

1. Bokhart MT, Muddiman DC. Infrared matrix-assisted laser desorption electrospray ionization mass spectrometry imaging analysis of biospecimens. *Analyst*. 2016;141(18):5236-5245. doi:10.1039/C6AN01189F
2. Hillenkamp F, Unsöld E, Kaufmann R, Nitsche R. A high-sensitivity laser microprobe mass analyzer. *Appl Phys*. 1975;8(4):341-348. doi:10.1007/BF00898368
3. Schürenberg M, Schulz T, Dreiswerd K, Hillenkamp F. Matrix-assisted laser desorption/ionization in transmission geometry: Instrumental implementation and mechanistic implications. *Rapid Commun Mass Spectrom*. 1996;10(15):1873-1880. doi:10.1002/(SICI)1097-0231(199612)10:15%3C1873::AID-RCM719%3E3.0.CO;2-3
4. Galicia MC, Vertes A, Callahan JH. Atmospheric pressure matrix-assisted laser desorption/ionization in transmission geometry. *Anal Chem*. 2002;74(8):1891-1895. doi:10.1021/ac011098i
5. Richards AL, Lietz CB, Wager-Miller JB, Mackie K, Trimpin S. Imaging mass spectrometry in transmission geometry. *Rapid Commun Mass Spectrom*. 2011;25(6):815-820. doi:10.1002/rcm.4927
6. Sampson JS, Hawkridge AM, Muddiman DC. Generation and detection of multiply-charged peptides and proteins by matrix-assisted laser desorption electrospray ionization (MALDESI) fourier transform ion cyclotron resonance mass spectrometry. *J Am Soc Mass Spectrom*. 2006;17(12):1712-1716. doi:10.1016/j.jasms.2006.08.003
7. Robichaud G, Barry JA, Muddiman DC. IR-MALDESI mass spectrometry imaging of biological tissue sections using ice as a matrix. *J Am Soc Mass Spectrom*. 2014;25(3):319-328. doi:10.1007/s13361-013-0787-6
8. Ovchinnikova OS, Bhandari D, Lorenz M, Van Berkel G. Transmission geometry laser ablation into a non-contact liquid vortex capture probe for mass spectrometry imaging. *Rapid Commun Mass Spectrom*. 2014;28(15):1665-1673. doi:10.1002/rcm.6946
9. Tu A, Muddiman DC. Internal energy deposition in infrared matrix-assisted laser desorption electrospray ionization with and without the use of ice as a matrix. *J Am Soc Mass Spectrom*. 2019;30(11):2380-2391. doi:10.1007/s13361-019-02323-2

10. Kibbe RR, Mellinger AL, Muddiman DC. Novel matrix strategies for improved ionization and spatial resolution using IR-MALDESI mass spectrometry imaging. *J Mass Spectrom*. 2022;57(8):e4875. doi:10.1002/jms.4875
11. Tu A, Muddiman DC. Systematic evaluation of repeatability of IR-MALDESI-MS and normalization strategies for correcting the analytical variation and improving image quality. *Anal Bioanal Chem*. 2019;411(22):5729-5743. doi:10.1007/s00216-019-01953-5
12. Bagley MC, Garrard KP, Muddiman DC. The development and application of matrix assisted laser desorption electrospray ionization: The teenage years. *Mass Spectrom Rev*. 2021;1-32. doi:10.1002/mas.21696
13. Knizner KT, Guymon JP, Garrard KP, et al. Next-generation infrared matrix-assisted laser desorption electrospray ionization source for mass spectrometry imaging and high-throughput screening. *J Am Soc Mass Spectrom*. 2022;57(6). doi:10.1002/jms.4869
14. Garrard KP, Ekelöf M, Khodjaniyazova S, Bagley MC, Muddiman DC. A versatile platform for mass spectrometry imaging of arbitrary spatial patterns. *J Am Soc Mass Spectrom*. 2020;31(12):2547-2552. doi:10.1021/jasms.0c00128
15. Ekelöf M, Manni JG Sr, Nazari M, Bokhart M, Muddiman DC. Characterization of a novel miniaturized burst-mode infrared laser system for IR-MALDESI mass spectrometry imaging. *Anal Bioanal Chem*. 2018;410(9):2395-2402. doi:10.1007/s00216-018-0918-9
16. Bagley MC, Ekelöf M, Muddiman DC. Determination of optimal electrospray parameters for Lipidomics in infrared-matrix-assisted laser desorption electrospray ionization mass spectrometry imaging. *J Am Soc Mass Spectrom*. 2020;31(2):319-325. doi:10.1021/jasms.9b00063
17. Chambers MC, Maclean B, Burke R, et al. A crossplatform toolkit for mass spectrometry and proteomics. *Nat Biotechnol*. 2012;30(10):918-920. doi:10.1038/nbt.2377
18. Race AM, Styles IB, Bunch J. Inclusive sharing of mass spectrometry imaging data requires a converter for all. *J Proteomics*. 2012;75(16):5111-5112. doi:10.1016/j.jprot.2012.05.035
19. Robichaud G, Garrard KP, Barry JA, Muddiman DC. MSiReader: An open-source Interface to view and analyze high resolving power MS imaging files on Matlab platform. *J Am Soc Mass Spectrom*. 2013;24(5):718-721. doi:10.1007/s13361-013-0607-z
20. Bokhart MT, Nazari M, Garrard KP, Muddiman DC. MSiReader v1.0: Evolving open-source mass spectrometry imaging software for targeted and untargeted analyses. *J Am Soc Mass Spectrom*. 2018;29(1):8-16. doi:10.1007/s13361-017-1809-6
21. Race AM, Bunch J. Optimisation of colour schemes to accurately display mass spectrometry imaging data based on human colour perception. *Anal Bioanal Chem*. 2015;407(8):2047-2054. doi:10.1007/s00216-014-8404-5
22. Nuñez JR, Anderton CR, Renslow RS. Optimizing colormaps with consideration for color vision deficiency to enable accurate interpretation of scientific data. *PLoS ONE*. 2018;13(7):e0199239. doi:10.1371/journal.pone.0199239
23. Palmer A, Phapale P, Chernyavsky I, et al. FDR-controlled metabolite annotation for high resolution mass spectrometry. *Nat Methods*. 2017;14(1):57-60. doi:10.1038/nmeth.4072
24. Jacobson RS, Thurston RL, Shrestha B, Vertes A. In situ analysis of small populations of adherent mammalian cells using laser ablation electrospray ionization mass spectrometry in transmission geometry. *Anal Chem*. 2015;87(24):12130-12136. doi:10.1021/acs.analchem.5b02971
25. Zavalin A, Todd EM, Rawhouser PD, Yang J, Norris JL, Caprioli RM. Direct imaging of single cells and tissue at sub-cellular spatial resolution using transmission geometry MALDI MS. *J Mass Spectrom*. 2012;47(11):1473-1481. doi:10.1002/jms.3132

SUPPORTING INFORMATION

Additional supporting information can be found online in the Supporting Information section at the end of this article.

How to cite this article: Joignant AN, Bai H, Guymon JP, Garrard KP, Pankow M, Muddiman DC. Developing transmission mode for infrared matrix-assisted laser desorption electrospray ionization mass spectrometry imaging. *Rapid Commun Mass Spectrom*. 2022;36(22):e9386. doi:10.1002/rcm.9386